J. Fluid Mech. (1997), *vol.* 331, *pp.* 145–167

Numerical studies of singularity formation at free surfaces and fluid interfaces in two-dimensional Stokes flow

By C. POZRIKIDIS

Department of Applied Mechanics and Engineering Sciences, University of California at San Diego, La Jolla, CA 92093-0411, USA

e-mail: costas@ames.ucsd.edu

(Received 13 May 1996 and in revised form 13 August 1996)

We consider the analytic structure of interfaces in several families of steady and unsteady two-dimensional Stokes flows, focusing on the formation of corners and cusps. Previous experimental and theoretical studies have suggested that, without surface tension, the interfaces spontaneously develop such singular points. We investigate whether and how corners and cusps actually develop in a time-dependent flow, and assess the stability of stationary cusped shapes predicted by previous authors. The motion of the interfaces is computed with high resolution using a boundary integral method for three families of flows. In the case of a bubble that is subjected to the family of straining flows devised by Antanovskii, we find that a stationary cusped shape is not likely to occur as the asymptotic limit of a transient deformation. Instead, the pointed ends of the bubble disintegrate in a process that is reminiscent of tip streaming. In the case of the flow due to an array of point-source dipoles immersed beneath a free surface, which is the periodic version of a flow proposed by Jeong & Moffatt, we find evidence that a cusped shape indeed arises as the result of a transient deformation. In the third part of the numerical study, we show that, under certain conditions, the free surface of a liquid film that is levelling under the action of gravity on a horizontal or slightly inclined surface develops an evolving corner or cusp. In certain cases, the film engulfs a small air bubble of ambient fluid to obtain a composite shape. The structure of a corner or a cusp in an unsteady flow does not have a unique shape, as it does at steady state. In all cases, a small amount of surface tension is able to prevent the formation of a singularity, but replacing the inviscid gas with a viscous liquid does not have a smoothing effect. The ability of the thin-film lubrication equation to produce mathematical singularities at the free surface of a levelling film is also discussed.

1. Introduction

There is a sufficient amount of experimental and theoretical evidence to suggest that, under certain conditions, the free surface of a liquid and the interface between two fluids may develop regions of high curvature, which have been described as apparent corners and cusps. In the theoretical limit where the surface tension vanishes, these regions become true corners and cusps both of which have infinite curvature and an associated discontinuity in the tangential plane. Several classes of Stokes flows where corner and cusp formation is either known or alleged to occur include the following.

(*a*) Flow past a two-dimensional or an axisymmetric bubble placed in an extensional or shear flow (e.g. Richardson 1968, 1973; Buckmaster 1972; Antanovskii 1994*b*, *c*).

The cusp on the free surface of a two-dimensional bubble immersed in an orthogonal stagnation-point flow is illustrated in figure 1(*a*).

(*b*) Flow inside a two-dimensional drop that is suspended in a gas and is shrinking under the action of a point sink located in its interior (Howison & Richardson 1995); and the complementary flow in the exterior of a bubble (Tanveer & Vasconelos 1994, 1995; Nie & Tanveer 1996). The cusp on the free surface of a shrinking drop is illustrated in figure 1(*b*).

(*c*) Flow near the meniscus of a liquid between two counter-rotating cylinders, and flow near the meniscus of a film plunging into a pool (Joseph *et al.* 1991; Jeong & Moffatt 1992; Joseph 1992). The first type of flow is depicted in figure 1(*c*).

(*d*) Flow near the free surface of a liquid whose motion is due to a point vortex or a point-vortex dipole immersed beneath the free surface (Joseph *et al.* 1991; Jeong & Moffatt 1992; Joseph 1992; Antanovskii 1994*a*). The periodic version of this flow is illustrated in figure 1(*d*).

(*e*) Flow due to the levelling of a liquid film on a horizontal surface, and flow of a deformed film down an inclined plane, depicted in figure 1(*e*, *f*). The formation of an interfacial singularity will be discussed in § 5.

A common feature of the aforementioned flows is the presence of a stagnation point precisely on, or near the free surface. The sharp curvature of the streamlines in the vicinity of the stagnation point seems to be a prerequisite for singularity formation. There are other types of interfacial singularities associated with pinching of layers or columns of fluid, accompanied by topological changes in geometry of an interface, but these will not concern us in this study (Tanveer & Vasconelos 1994; Nie & Tanveer 1996).

The majority of previous theoretical and computational studies on the structure of interfacial corners and cusps have considered steady flows. One can make an important distinction between (*a*) two-dimensional and (*b*) three-dimensional or axisymmetric flow. In the first case, the velocity at the location of a corner or cusp with non-zero surface tension takes an infinite value, whereas in the second case it is finite (Richardson 1968). Corners and cusps in two-dimensional flow are thus expected to occur only in the theoretical limit of vanishing surface tension. This rather strong requirement appears to diminish the significance of, and has been an impediment for, theoretical investigations. But describing the way in which a singularity is formed as the surface tension is diminished has proven to be both an illuminating and fruitful approach. Jeong & Moffatt (1992), in particular, explicitly demonstrated that a two-dimensional free surface with a cusped shape is mathematically consistent and physically acceptable in the context of Stokes flow and probably Navier–Stokes flow. The existence of a stationary cusped shape, however, does not guarantee its spontaneous formation in an unsteady flow; the issue of stability is yet to be addressed.

In recent years, several authors have developed semi-analytical and numerical methods for computing the evolution of two-dimensional and axisymmetric bubbles and drops leading to cusped shapes. Their work is based on complex-variable formulations and boundary-integral methods for Stokes flow. Antanovskii (1994*b*, *c*) described the evolution of a two-dimensional bubble suspended in an incident extensional flow; Tanveer & Vasconelos (1994, 1995) and Nie & Tanveer (1996) considered flows exterior to a shrinking two-dimensional or axisymmetric bubble; Howison & Richardson (1995) considered the complementary problem of flow inside a two-dimensional shrinking drop. The last authors cleverly argue that, without surface tension, the spontaneous occurrence of a singularity along the free surface of a shrinking drop with an arbitrary initial shape is a consequence of the reversibility of

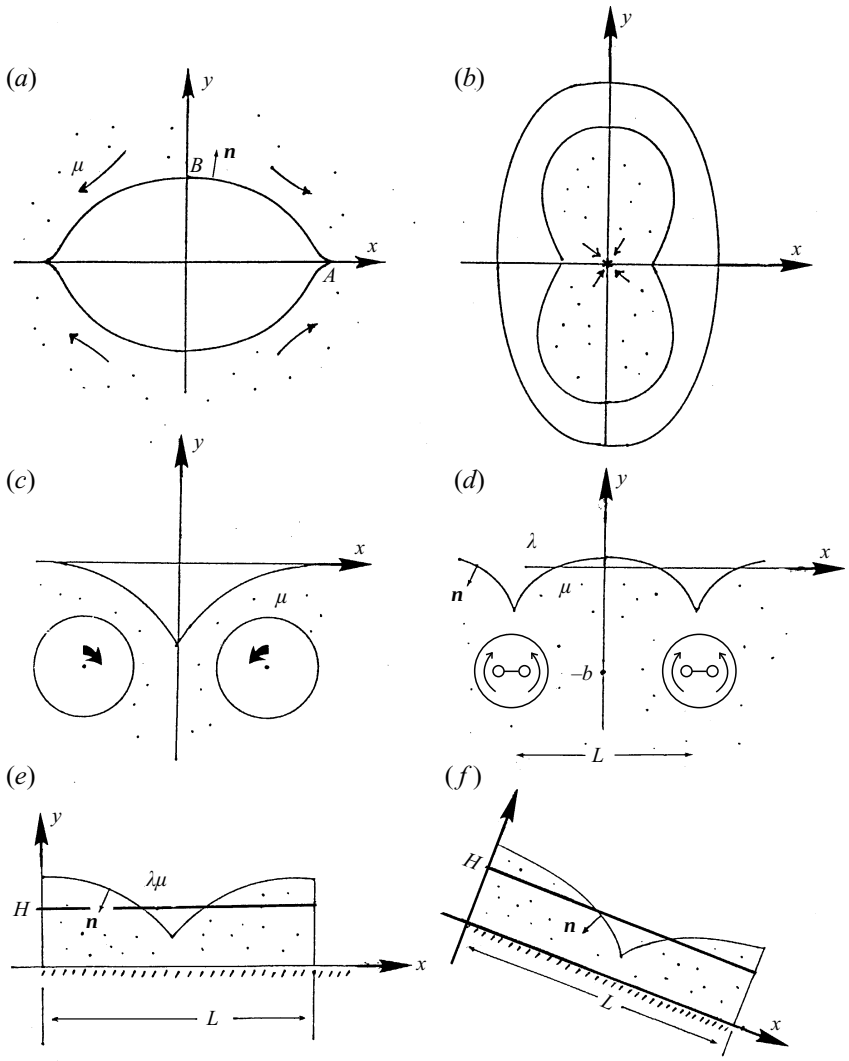

FIGURE 1. Schematic illustration of six types of Stokes flows involving free surfaces and fluid with corners and cusps. (*a*) Flow past a two-dimensional bubble placed in an extensional flow; (*b*) flow inside of a two-dimensional drop that is suspended in a gas and is shrinking under the action of a point sink located in its interior; (*c*) flow near the meniscus of a liquid between two counter-rotating rollers; (*d*) flow near the free surface of a liquid whose motion is due to a periodic array of immersed point vortices or point-vortex dipoles; (*e*) flow due to the levelling of a liquid film on a horizontal surface; (*f*) flow of a deformed film down an inclined plane.

Stokes flow. If the whole of the fluid were drained through the point sink, reversing the flow at the late stages of drainage would produce a drop with a circular shape.

There have been three additional numerical investigations of unsteady flows leading to formation of cusps. Joseph *et al.* (1991) used a numerical software package based on a finite-element method to compute the evolution of the free surface of a liquid placed within a rectangular computational box, with a specified inlet and outlet. The streamline pattern of this model flow includes a stagnation point at the undeformed free surface, which causes a symmetric depression. In the absence of surface tension, the computations became unstable after a finite time of evolution; at that point, the

free surface had already developed a region of high curvature. The breakdown of the numerical method was regarded as evidence of cusp formation. When the surface tension was set to a non-zero value, the free surface was seen to obtain a smooth steady shape. Joseph (1992) discussed the results of an unpublished report by Palmquist & Kistler on the flow due to the plunging of a liquid film into a pool, conducted using a finite-element method. Cusp formation was established by extrapolating results for finite but small surface tension. Finally, Koplik & Banavar (1994) carried out molecular dynamics simulations of the flow between two counter-rotating rollers. Their results cast a shadow of doubt on the physical relevance of cusp formation predicted in the context of continuum mechanics, but an alternative explanation for these discrepancies will emerge from our discussion.

The numerical results of all the aforementioned authors confirm that a cusp may indeed form in a spontaneous manner in an unsteady flow. But, mainly due to difficulties with the accuracy of the numerical methods, the actual process of singularity formation and the shape of computed evolving cusps have not been described in satisfactory detail. Joseph (1992) convincingly argued that the geometry of a steady cusp must be describable by a certain power law, and his theory is in agreement with the exact solution of Jeong & Moffatt (1992). On the other hand, Howison & Richardson (1995) perceptively pointed out that reversibility of Stokes flow allows an evolving corner or cusp to take any arbitrary shape. The relation between the cusps developing in an unsteady flow and the stationary cusps analysed by Richardson, Jeong & Moffatt, and Joseph for steady flow is not clear. Finally, to this author's knowledge, the formation of a corner in either a steady or an unsteady two-dimensional Stokes flow has not been reported, although its existence has been discussed.

In this paper, we report the results of numerical computations on four families of interfacial flows leading to the formation of corners and cusps. In §3, we study the evolution of a bubble in a straining flow invented by Antanovskii (1994*c*), illustrated in figure 1(*a*), and in §4, we consider the periodic version of the Jeong–Moffatt flow, depicted in figure 1(*d*). In both cases, previous solutions of the steady flow problem without surface tension have suggested the spontaneous formation of cusps. We investigate whether and how these cusps actually form during an unsteady deformation beginning with different initial shapes.

In §5, we study the levelling of a non-planar liquid film evolving on a horizontal or inclined surface, shown in figure 1(*e*, *f*), and observe the spontaneous occurrence of corners and cusps. This flow has been considered both theoretically and numerically on many previous occasions but, surprisingly, it has not been identified as a host of singularity formation. When the film thickness is sufficiently small compared to the wavelength of the perturbation, the evolution of the film thickness is described by the equations of lubrication flow. We show that this simplified description cannot capture the precise process of singularity formation, although it may produce other types of singular behaviour.

We conclude in §6 by summarizing the results and drawing attention to the analogous problem of interfacial singularity formation in the Hele–Shaw cell.

2. Mathematical formulation and numerical method

The investigations are based on numerical solutions of the equations of Stokes flow using boundary-integral methods. The development of the integral representation is straightforward (e.g. Pozrikidis 1992), and we confine this discussion to presenting the

final integral equations and outlining the numerical procedure for the four classes of flows illustrated in figure 1(*a*, *d–f*).

For all flows, we trace the interface – and for periodic flow one period of it – with a set of marker points that move either with the velocity of the fluid, or with the component of the velocity of the fluid that is normal to the interface, and advance the position of the points using the first- or second-order Runge–Kutta method. The time step is either kept constant or adjusted in the course of the computation according to the minimum radius of curvature of the free surface, as will be discussed in §4; this provides us with an effective method of capturing singularity formation.

The velocity of the fluid at the free surface is computed by solving a Fredholm integral equation of the second kind. To improve the accuracy of the results and the efficiency of the numerical method, we produce the solution by the method of fixed-point iterations. In certain cases, convergence requires deflating the spectrum of the double-layer integral of Stokes flow, so as to make its spectral radius less than unity, as will be described in the following subsections.

2.1. *Deformation of a bubble or drop*

For flow past a bubble or drop, illustrated in figure 1(*a*), we compute the interfacial velocity by solving the integral equation

$$u_j(\boldsymbol{x}_0) = \alpha u_j^{\infty}(\boldsymbol{x}_0) - \frac{\alpha}{4\pi\mu}\int_S \Delta f_i(\boldsymbol{x})\, G_{ij}(\boldsymbol{x},\boldsymbol{x}_0)\,\mathrm{d}l(\boldsymbol{x}) + \frac{\beta}{2\pi}\int_S^{\mathrm{PV}} u_i(\boldsymbol{x})\, T_{ijk}(\boldsymbol{x},\boldsymbol{x}_0)\, n_k(\boldsymbol{x})\,\mathrm{d}l(\boldsymbol{x}) - \frac{\beta}{\chi} n_j(\boldsymbol{x}_0)\int_S u_i(\boldsymbol{x})\, n_i(\boldsymbol{x})\,\mathrm{d}l(\boldsymbol{x}), \quad (2.1)$$

where $\boldsymbol{u}^{\infty}$ is the velocity of the incident flow to be given a specific form in §3, $\boldsymbol{n}$ is the unit normal vector pointing out of the bubble, $\alpha = 2/(1+\lambda)$, $\beta = (1-\lambda)/(1+\lambda)$, and λ is the ratio of the viscosity of the fluid occupying the bubble to the viscosity of the ambient liquid μ; for the inviscid bubble considered in the main part of this study, $\lambda = 0$. The quantities $\boldsymbol{G}$ and $\boldsymbol{T}$ are the two-dimensional Stokeslet and its associated stress tensor, S is the interface, χ is the instantaneous total arclength of the interface, and PV designates the principal value of the double-layer integral.

In this problem, we neglect the effects of gravity and set the discontinuity in the interfacial traction $\Delta\boldsymbol{f}$ equal to $\gamma\kappa\boldsymbol{n}$, where γ is the surface tension, and κ is the curvature of the interface in the (x, y)-plane. Since the free surface is in dynamic equilibrium, the total force exerted by the bubble on the ambient fluid is equal to zero, and the disturbance flow decays far from the interface preventing the well-known divergent behaviour of unbounded two-dimensional Stokes flow.

It is worth noting, parenthetically, that the non-symmetric version of the flow depicted in figure 1(*b*), without the symmetries with respect to the x- and y-axes, would seemingly require the presence of a point force and a rotlet at the position of the point source in order to balance the force and the torque exerted by the interface on the liquid (Howison & Richardson 1995). But since the free surface is in equilibrium, the total force exerted on it by surface tension vanishes and a point force is not required. The presence of a rotlet, however, seems to be imperative.

In the numerical implementation, we consider an incident flow that is symmetric with respect to the x- and y-axes, and require a corresponding symmetry for the free surface. Accordingly, we compute the velocity over one quarter of the interface, and set the velocity over the remainder by reflection. This practice effectively eliminates the eigenfunctions of the double-layer potential expressing rigid-body motion. The last

term in equation (2.1) deflates the spectrum of the double-layer operator be removing its marginal eigenvalue, and thus allows an iterative solution. In practice, only a few iterations are necessary in order to obtain a solution that is accurate to the fifth decimal place.

2.2. *Deformation of an interface due to a periodic array of point-source dipoles*

Next, we consider a semi-infinite pool of a liquid whose interface deforms under the action of a periodic array of point-source dipoles pointing along the y-axis, each of strength δ, as shown in figure 1(d). The singularities are immersed beneath the interface at a distance b, and are separated by the distance L. Note that a point-source dipole pointing along the y-axis may also be interpreted as a point-vortex dipole pointing along the x-axis.

To facilitate the mathematical formulation, we decompose the velocity $\boldsymbol{u}$ into the velocity due to the point-source dipoles $\boldsymbol{u}^{\infty}$, and a disturbance velocity $\boldsymbol{u}^{D}$. The disturbance velocity at the interface is computed by solving the integral equation

$$u_j^D(\boldsymbol{x}_0) = -\frac{\alpha}{4\pi\mu}\int_S (\Delta f_i(\boldsymbol{x}) - (1-\lambda) f_i^{\infty}(\boldsymbol{x}))\, G_{ij}^{1P}(\boldsymbol{x},\boldsymbol{x}_0)\, \mathrm{d}l(\boldsymbol{x}) + \frac{\beta}{2\pi}\int_S{}^{\mathrm{PV}} u_i^D(\boldsymbol{x})\, T_{ijk}^{1P}(\boldsymbol{x},\boldsymbol{x}_0)\, n_k(\boldsymbol{x})\, \mathrm{d}l(\boldsymbol{x}), \quad (2.2)$$

where $\boldsymbol{f}^{\infty}$ is the traction at the interface corresponding to the unperturbed flow due to the singularities, λ is the ratio of the viscosities of the upper and lower fluid, and $\boldsymbol{G}^{1P}$, $\boldsymbol{T}^{1P}$ are the singly periodic Stokeslet and its associated stress tensor derived in closed form by Pozrikidis (1992). The effects of gravity are neglected by setting the discontinuity in the interfacial traction $\Delta\boldsymbol{f}$ equal to $\gamma\kappa\boldsymbol{n}$. The rest of the symbols were defined in the preceding subsection. For the liquid pool underneath an inviscid gas considered in the main part of our numerical study, $\lambda = 0$. A closed-form expression for the velocity of the incident $\boldsymbol{u}^{\infty}$ can be found in standard texts of fluid mechanics (e.g. Pozrikidis 1997*a*).

It is worth noting again that, because the total force and torque exerted on one period of the interface by the traction field $\Delta\boldsymbol{f}$ vanishes, the presence of point forces or rotlets at the location of the point-source dipoles is not required.

2.3. *Integral equation for the levelling of a horizontal film*

In the third case study, we consider the levelling of a periodic liquid film with viscosity μ lying on a horizontal surface, underneath another viscous fluid with viscosity $\lambda\mu$, as illustrated in figure 1(e). The velocity at the free surface is obtained by solving the integral equation

$$u_j(\boldsymbol{x}_0) = -\frac{\alpha}{4\pi\mu}\int_S \Delta f_i(\boldsymbol{x})\, G_{ij}^{1PW}(\boldsymbol{x},\boldsymbol{x}_0)\, \mathrm{d}l(\boldsymbol{x}) + \frac{\beta}{2\pi}\int_S{}^{\mathrm{PV}} u_i(\boldsymbol{x})\, T_{ijk}^{1PW}(\boldsymbol{x},\boldsymbol{x}_0)\, n_k(\boldsymbol{x})\, \mathrm{d}l(\boldsymbol{x}) - \frac{\beta}{\chi} n_j(\boldsymbol{x}_0)\int_S u_i(\boldsymbol{x})\, n_i(\boldsymbol{x})\, \mathrm{d}l(\boldsymbol{x}), \quad (2.3)$$

where $\Delta\boldsymbol{f} = (\gamma\kappa + \Delta\rho g(y-H))\,\boldsymbol{n}$, $\Delta\rho$ is the difference of the densities of the film and overlying fluid, g is the magnitude of the acceleration due to gravity, $y = H$ describes the location of the free surface of the flat film. The kernels $\boldsymbol{G}^{1PW}$ and $\boldsymbol{T}^{1PW}$ are the singly periodic Green's function and its associated stress tensor for flow due to a periodic array of point forces in the presence of a flat wall (Pozrikidis 1992). The rest of the symbols were defined in the preceding subsections.

2.4. *Integral equation for the evolution of an inclined film*

To develop the boundary-integral formulation for the flow of the inclined film depicted in figure 1(*f*), we decompose the velocity $\boldsymbol{u}$ into the sum of the unperturbed velocity $\boldsymbol{u}^{\infty}$ corresponding to the flat-film solution, and a disturbance velocity $\boldsymbol{u}^{D}$; for the horizontal film discussed in the preceding subsection, $\boldsymbol{u}^{\infty} = \boldsymbol{0}$. The disturbance velocity at the interface is computed by solving the integral equation

$$u_j^D(\boldsymbol{x}_0) = -\frac{\alpha}{4\pi\mu}\int_S (\Delta f_i(\boldsymbol{x}) - f_i^{\infty}(\boldsymbol{x}))\, G_{ij}^{1PW}(\boldsymbol{x},\boldsymbol{x}_0)\,\mathrm{d}l(\boldsymbol{x}) + \frac{\beta}{2\pi}\int_S{}^{\mathrm{PV}}\, u_i^D(\boldsymbol{x})\, T_{ijk}^{1PW}(\boldsymbol{x},\boldsymbol{x}_0)\, n_k(\boldsymbol{x})\,\mathrm{d}l(\boldsymbol{x}) - \frac{\beta}{\chi} n_j(\boldsymbol{x}_0)\int_S u_i(\boldsymbol{x})\, n_i(\boldsymbol{x})\,\mathrm{d}l(\boldsymbol{x}). \quad (2.4)$$

The quantity $\boldsymbol{f}^{\infty}$ is the traction at the interface corresponding to the flow $\boldsymbol{u}^{\infty}$, with components

$$f_x^{\infty} = -\Delta\rho(y-H)\,(g_y n_x + g_x n_y), \quad f_y^{\infty} = -\Delta\rho(y-H)\,\boldsymbol{g}\cdot\boldsymbol{n}, \quad (2.5)$$

where $\Delta\rho$ is the density difference between the film liquid and the overlying fluid, $y = H$ describes the free surface of the flat film, $\boldsymbol{g}$ is the gravitational acceleration vector, and $\boldsymbol{n}$ is the unit normal vector pointing into the film. Finally, the discontinuity in the interfacial traction is given by $\Delta\boldsymbol{f} = \gamma\kappa\boldsymbol{n}$.

2.5. *Adaptive point redistribution*

An important component of the numerical method is an adaptive point redistribution algorithm that allows us to describe the fine features of the evolving interface. After each time step, we examine the distribution of the marker points, and compute (*a*) the angle that is subtended by each circular arc that passes through successive triplets of marker points, and (*b*) the separation between two successive points. If the angle is too large, we replace the middle point with two evenly spaced points; if the separation is too large, we introduce a point in the middle; and if the separation is too small, we replace the two successive points by a point in the middle. The last operation is possible only if the resulting point distribution does not violate the first two criteria. Appropriate modifications are made for the points that lie in the neighbourhood of a plane of symmetry, such as the $y = 0$ or $x = 0$ plane in figure 1(*a*), so that the point distribution respects the symmetry of the flow at all times.

2.6. *Numerical implementation and performance*

In the numerical procedure, we approximate the interface with the union of circular arcs that are subtended between successive triplets of marker points. The radius of curvature at each point is approximated by the radius of the arc, with a negative sign when the marker points rotate in the clockwise direction along an arc. Cubic-spline interpolation was implemented but did not have a significant enough effect on the accuracy of the results to justify the additional expense.

The discontinuity in the interfacial traction $\Delta\boldsymbol{f}$ and interfacial velocity were assumed to vary in a linear manner with respect to arclength over each arc. To compute the single-layer integral, we subtract the logarithmic singularity of the integrand, and integrate it analytically over each arc. The double-layer integral of two-dimensional Stokes flow is non-singular when it is integrated over an element with a smooth shape, and does not require a special treatment. The non-singular integrals are computed using six-point Gauss–Legendre quadrature. Picard iterations are carried out based on

a projection matrix that is constructed using a finite-difference method. The iteration time was a small fraction of the time necessary to compute the single-layer potential or for constructing the projection matrix.

All computations were performed on a Sun Sparcstation 20, with a minimum of 64 points along the interface. The maximum CPU time for a complete run was less than two hours. The area of a bubble, drop, or liquid layer was preserved with an error that is less than 0.01% up to the completion of each computation.

3. Bubble deformation in a straining flow

Richardson (1968, 1973) developed an elegant method for computing the steady shape of a two-dimensional inviscid bubble immersed in a purely straining flow, a simple shear flow, and a parabolic flow; in the third case the bubble may be placed at an off-centre position. His method was based on a complex-variables formulation of Stokes flow. In the first two cases of purely straining and simple shear flow, he found that there is a critical value of the capillary number $Ca = 2\mu Ga/\gamma$ above which a steady shape cannot be established, and the bubble continues to elongate; G is the shear rate or rate of elongation of the incident flow, and a is the equivalent bubble radius. At sub-critical values of the capillary number, the bubble assumes a perfectly elliptical shape.

The behaviour of a two-dimensional bubble in a purely straining flow is in sharp contrast to the corresponding behaviour of an axisymmetric bubble in an extensional uniaxial flow. The latter retains a compact shape at all values of the capillary number, and it is apparently able to do so by developing pointed ends with large curvature. In the theoretical limit where the surface tension vanishes, the pointed ends obtain conical shapes. Unfortunately, it has not been possible to describe the precise structure of the flow in the vicinity of these singular points (Buckmaster 1972).

The intriguing differences in the behaviour of axisymmetric and two-dimensional bubbles in straining flow motivated Antanovskii (1994*b*, *c*) to study the deformation of a two-dimensional bubble in a general class of incident straining flows. In the first part of his study, Antanovskii used the complex-variable formulation to study the *transient* deformation of a bubble in various types of irrotational incident flows, including flows whose complex potential is an integral power of the complex variable z. When the value of the exponent is equal to 2, the incident flow reduces to the purely extensional flow studied earlier by Richardson (1968). Antanovskii (1994*b*) computed evolutions from the circular shape at finite values of the capillary number, and found that, in all cases, the bubble deforms and obtains a nearly cusped shape. Numerical inaccuracies prevented him from analysing the behaviour at long times for zero surface tension where a true cusp allegedly forms.

More relevant to this discussion is the second part of Antanovskii's (1994*c*) work on the steady shape of a bubble immersed in a purely straining orthogonal stagnation-point flow. An important new feature is that the incident flow also has a small rotational component. With the centre of the bubble placed at the origin, the velocity field of the incident flow is given by

$$\left.\begin{aligned} u_x^\infty &= \frac{G}{a^2}x(a^2+2c_1(x^2-3y^2)+c_2(x^2+3y^2)),\\ u_y^\infty &= -\frac{G}{a^2}y(a^2+2c_1(3x^2-y^2)+c_2(3x^2+y^2)),\end{aligned}\right\} \tag{3.1}$$

where G is the rate of extension, a is the bubble equivalent radius, and c_1, c_2, are two

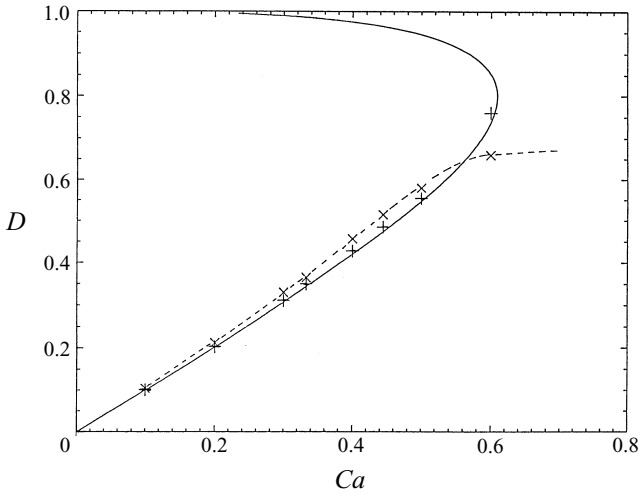

FIGURE 2. The dependence of the bubble deformation parameter $D = (A-B)/(A+B)$, where A and B are the half-lengths of the bubble along the x- or the y-axis as shown in figure 1 (a), on the capillary number. The solid line was drawn from Richardson's analytical solution for an orthogonal stagnation-point flow corresponding to $c_1 = 0$, $c_2 = 0$, and the + correspond to the present numerical results. The dashed line tracing the data plotted with × shows numerical results for a flow with $c_1 = 0$, $c_2 = 0.05$.

dimensionless parameters; setting $c_1 = 0$ and $c_2 = 0$ yields irrotational orthogonal stagnation-point flow.

Antanovskii (1994*c*) computed families of steady bubble shapes for various combinations of c_1 and c_2, and found that, at sufficiently large positive values of either one of these parameters, steady bubble shapes exist for all values of the capillary number. When this occurs, as the capillary number is increased the bubbles tend to develop pointed ends with cusped shapes. This behaviour is similar to that of axisymmetric bubbles placed in a purely elongational flow studied by Buckmaster (1972). An important difference is that the axisymmetric bubbles develop conical instead of cusped ends.

3.1. *Results and discussion*

We want to investigate the process of cusp formation during the transient phase where a bubble starts deforming from a specified initial shape.

Our numerical results for $c_1 = 0$ and $c_2 = 0$ are in excellent agreement with the analytical results of Richardson (1973); and this confirms the reliability of the numerical method. In figure 2 we illustrate the dependence of the bubble deformation parameter D on the capillary number, where $D = (A-B)/(A+B)$, and A, B are the half-lengths of the bubble along the x- or y-axis, as shown in figure 1 (a). The solid line in figure 2 was drawn using Richardson's analytical solution, and the plusses represent numerical results obtained with 32–60 points around a quarter of the interface. The asymptotic value of the deformation parameter was computed using the method of Aitken extrapolation (e.g. Pozrikidis 1997*b*), which is based on the verifiable assumption that the interface approaches its asymptotic value at an exponential rate.

The numerical results show that there is a critical value of Ca above which the bubble continues to elongate and does not reach a steady shape, in excellent agreement with Richardson's predictions that place the critical value at 0.609. For each sub-critical value of the capillary number, there are two steady bubble shapes; the one corresponding to the large deformation is unstable and cannot be realized. The steady

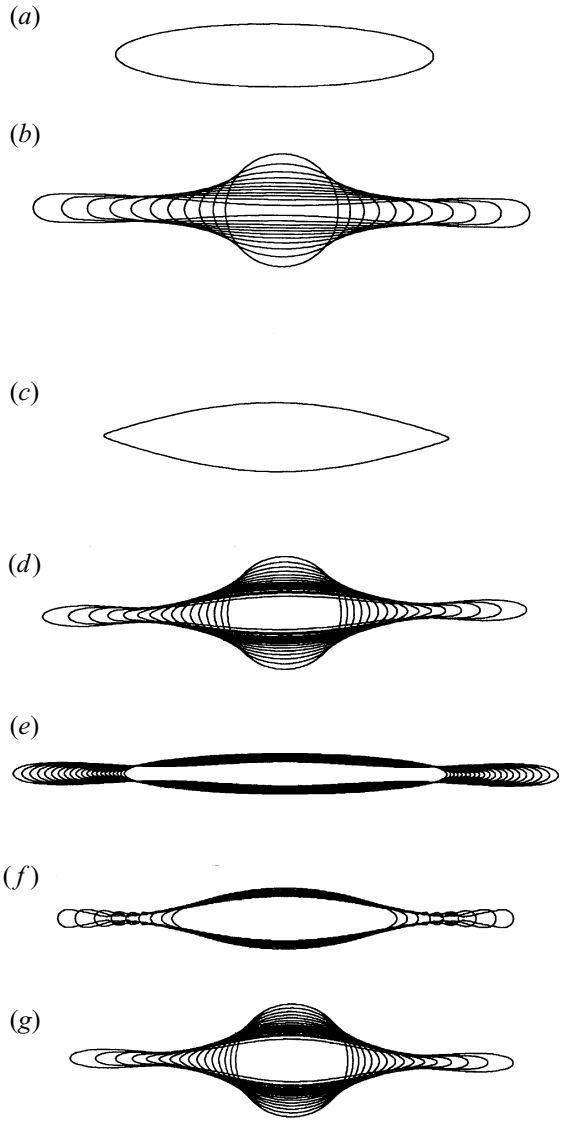

FIGURE 3. (*a*) The shape of a stationary bubble, and (*b*) the evolving shape of a bubble in an orthogonal stagnation-point irrotational flow, corresponding to $c_1 = 0$, $c_2 = 0$, for $Ca = 0.6$ and ∞. (*c*) The shape of a stationary bubble, and (*d–f*) the evolving shape of a bubble in a flow with $c_1 = 0$, $c_2 = 0.05$, for $Ca = 0.6$ and ∞. (*g*) The evolving shape of a circular bubble in a flow with $c_1 = 0.05$, $c_2 = 0$, for $Ca = \infty$.

shape of a bubble for $Ca = 0.6$, and the continued deformation of a bubble with vanishing interfacial tension corresponding to $Ca = \infty$, both for $c_1 = 0$ and $c_2 = 0$, are shown, respectively, in figure 3(*a*, *b*).

To investigate the effect of the rotational component of the incident flow, we consider, as a case study, a flow with $c_1 = 0$ and $c_2 = 0.05$. Antanovskii (1994*c*) found that steady bubble shapes exist at all values of the capillary number. As the surface tension is decreased, the bubble elongates and tends to develop pointed ends which eventually assume cusped shapes. The curvature of the interface at the tip increases in an exponential manner with respect to the capillary number.

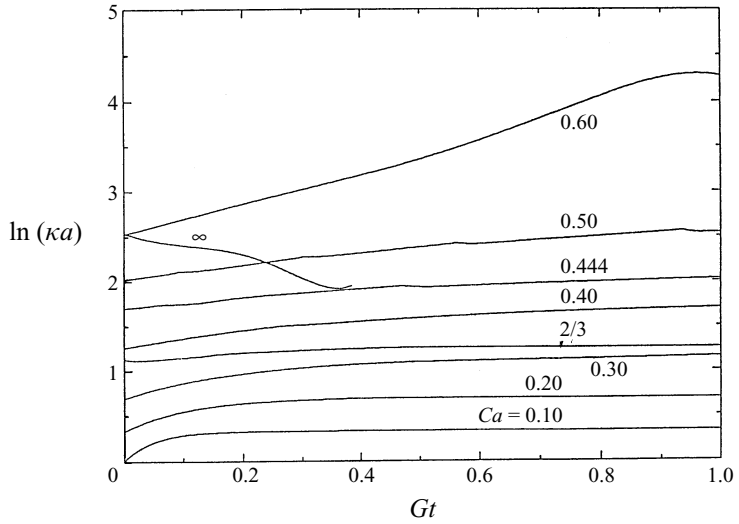

FIGURE 4. Evolution of the curvature of the free surface at the tip of a bubble, for an incident flow with $c_1 = 0$, $c_2 = 0.05$, at several values of the capillary number.

Our numerical results at small and moderate values of the capillary number are in excellent agreement with Antanovskii's predictions. In figure 2 we plot, with a dashed line tracing the numerical data indicated by the symbol $\times$, the asymptotic deformation D computed using the method of Aitken extrapolation, and obtain excellent agreement with Antanovskii's (1994*c*) results read from the graph in his figure 7. The D–Ca curve rises and then tends to become horizontal yielding stationary shapes for any finite value of Ca.

The steady shape of a bubble with $Ca = 0.6$, $c_1 = 0$ and $c_2 = 0.05$ is shown in figure 3(*c*). The contrast with the shape shown in figure 3(*a*) corresponding to an irrotational straining flow, is evident. The radius of curvature of the bubble at the pointed ends has a very small value, and this appears to corroborate Antanovskii's predictions that a cusped shape will form in the absence of interfacial tension. It may appear from figure 3(*c*) that a corner instead of a cusp is likely to form at infinite capillary number, but profiles plotted by Antanovskii show that the interior angle actually decreases to zero to yield a cusp.

To investigate the process of cusp formation, we computed the transient deformation of a bubble with vanishing surface tension, starting from several different initial shapes. Results of three such computations are shown in figure 3(*d–f*). In figure 3(*d*), the initial bubble shape is a circle; in figure 3(*e*), the initial shape is an ellipse with aspect ratio equal to 8, which corresponds to a deformation parameter that is close to that predicted by Antanovskii (1994*c*) for a cusped bubble; and in figure 3(*f*), the initial shape is the steady shape for a finite value of the capillary number. In all cases, and in others computed but not shown, the bubble behaves in a similar manner: It elongates along the x-axis, and it develops a dimple near the tip in a process that can be described as tip streaming. The upper and lower parts of the interface cross soon after the last stage shown in figure 3(*f*), indicating bubble breakup in the manner described by Tanveer & Vasconelos (1994, 1995) for a shrinking bubble.

Additional insights into the transient motion of a bubble can be obtained by considering the evolution of the curvature of the interface at the tip, shown in figure 4. In these series of computations, the initial shape of a bubble at a particular value of

the capillary number was taken to be the steady shape at a somewhat smaller value. The asymptotic approach to a steady value is evident in all cases except when $Ca = \infty$ corresponding to figure 3(*f*). In this case, the curvature at the tip decreases with time, reflecting the process of tip streaming.

Similar results were obtained for other values of c_1 and c_2 considered by Antanovskii (1994*c*). For example, figure 3(*g*) illustrates the evolution of a bubble from a circular shape in a flow with $c_1 = 0.05$ and $c_2 = 0$, in the absence of surface tension. Antanovskii's computations predict a stationary bubble with a cusped shape; we find that the bubble exhibits continued elongation, suggesting that the cusped configuration is either unstable or can be reached only from a narrow window.

4. Deformation of a free surface in the periodic Jeong–Moffatt flow

Jeong & Moffatt (1992) studied the deformation of the free surface of a semi-infinite pool of a liquid, due to an immersed two-dimensional point-source or point-vortex dipole. The periodic version of this flow is illustrated in figure 1(*d*). Remarkably, these authors were able to find an exact solution for steady flow, and describe the shape of the deformed free surface in closed analytical form. Their results demonstrated that the maximum curvature of the free surface, occurring at the point of maximum depression, is an exponentially increasing function of the capillary number.

Jeong & Moffatt found that, when the surface tension vanishes, the free surface develops a cusp that is described by the form $x - x_c = c(y - y_c)^{3/2}$, where x_c is the position of the cusp, the x-axis is perpendicular to the plane of symmetry, and c is a constant, in agreement with the earlier predictions of Joseph *et al.* (1991). The flow near the cusp was discussed further by Joseph (1992). Antanovskii (1994*a*) extended the formulation of Jeong & Moffatt to include the effects of a surfactant, but an exact solution could no longer be obtained.

Our objective is to investigate the process of cusp formation during the transient phase, as the free surface starts deforming from a specified initial shape. To facilitate the numerical solution, we extend the flow of Jeong & Moffatt to its periodic version, as discussed in §2. Jeong & Moffatt showed that gravity plays a secondary role in the structure of the flow near the trough of the free surface; accordingly, we neglect it in our formulation.

The transient motion and asymptotic shape of the free surface is a function of capillary number $Ca = \mu\delta/b^2\gamma$, where δ is the strength of the dipoles, and the rest of the variables were defined in §2 or figure 1(*d*). Jeong & Moffatt used the alternative capillary number $\mathscr{C} = \mu\alpha/d^2\gamma$, where $\alpha = \delta/(2\pi)$, $d = b + y_{Max}$, and y_{Max} is the maximum elevation of the free surface. The two capillary numbers are related by $\mathscr{C} = Ca\, b^2/(2\pi d^2)$.

When the capillary number vanishes, the free surface is flat; when it has a finite value, the free surface dips down above the singularities and settles to a steady shape. Steady free-surface shapes for $Ca = 0.5$ and 1 are shown in figure 5(*a*), for $L/b = 4$. In both cases, the free surface has a nearly flat initial shape with a small sinusoidal undulation. The corresponding evolutions of the maximum curvature of the free surface, occurring at the trough, are illustrated on a linear-log scale in figure 5(*b*). For $Ca = 0.25$, 0.50, 2/3, and 1.0, the curvature tends to a constant value that spans nearly two orders of magnitude. This behaviour is consistent with the exponential dependence of the maximum curvature on Ca demonstrated by Jeong & Moffatt and physically explained by Hinch in an Appendix to their paper. Unfortunately, the accuracy of our numerical results near the steady state severely worsens as the capillary number is

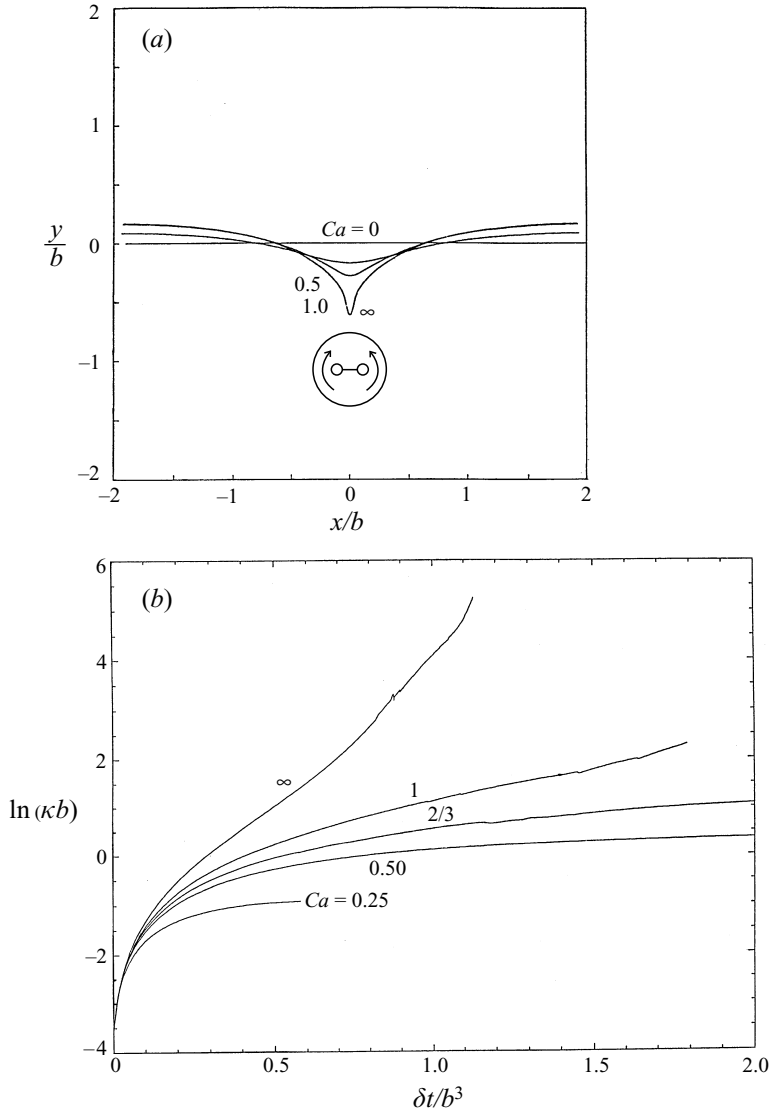

FIGURE 5. (*a*) Steady free-surface shapes in the periodic Jeong–Moffatt flow with $L/b = 4$, for $Ca = 0$, 0.5, 1.0, ∞. (*b*) Evolution of the free-surface curvature at the trough, κ, for several values of Ca.

raised, and this prevented us from examining the precise relationship between the maximum curvature and the capillary number in more detail.

When the surface tension vanishes and capillary number becomes infinite, the numerical results show that the curvature at the trough increases without limit, and tends to become infinite at a *finite* time, yielding a cusp. Figure 6(*a*) shows the detailed shape of the evolving free surface near the trough, at a sequence of time instants near the critical time where a cusp is about to form. In the numerical method, in order to capture the process of cusp formation, we adjust the time step in an adaptive manner. After extensive experimentation with different methods – including the implementation of a Runge–Kutta–Fehlberg RKF23 method with several error estimators – best results

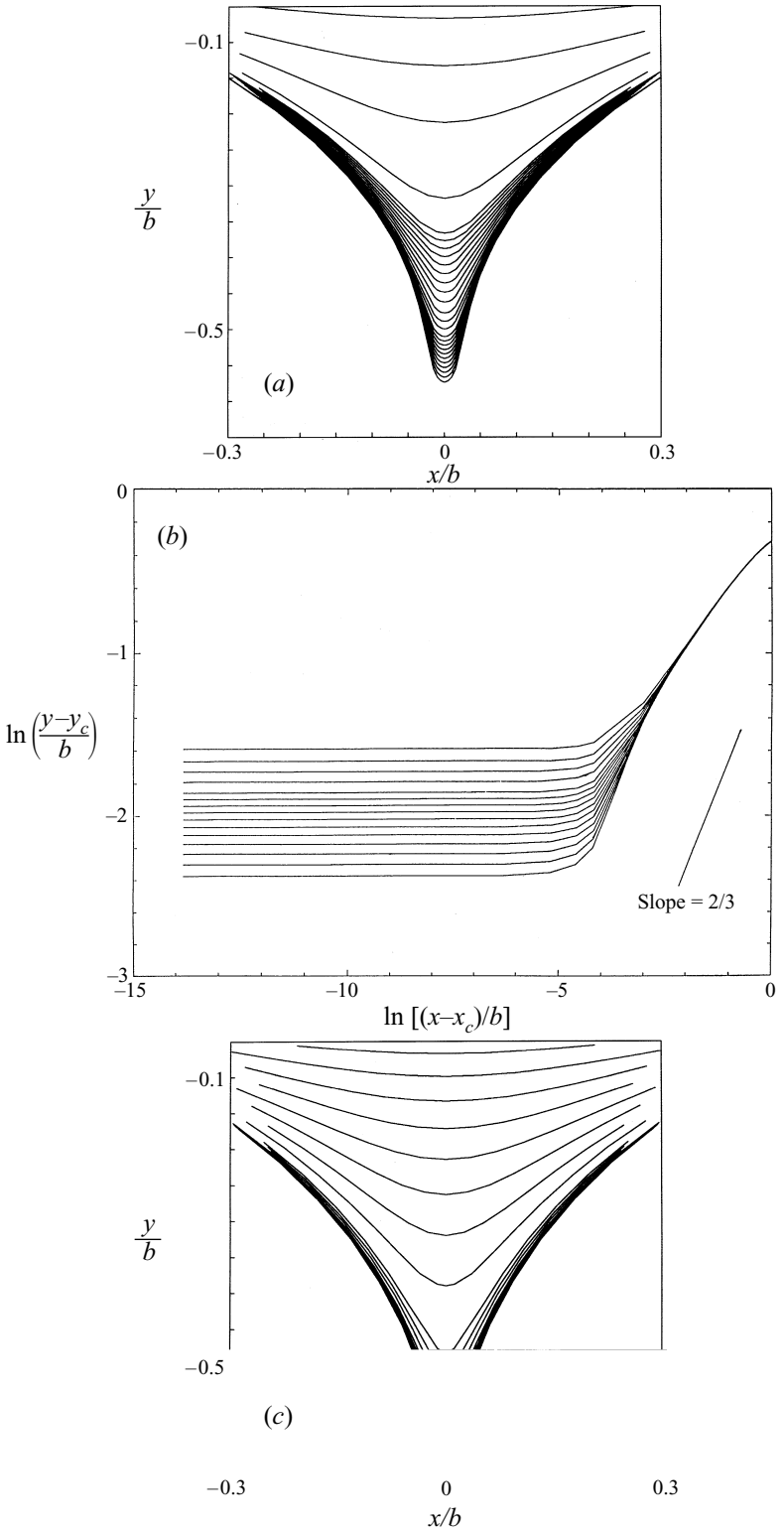

FIGURE 6. For caption see facing page.

were obtained when the adjustment was such that the curvature at the trough increases by a preset amount over each time step. The maximum increment was set equal to $2/b$ or $5/b$. When the time step is kept constant during the integration, the interface crosses itself, causing the numerical method to break down at a finite time. Taking into consideration that maintaining the time step constant did not cause any such difficulties in the problem of bubble deformation discussed in the preceding section, we regard this failure as evidence of cusp formation.

For the particular conditions corresponding to figure 6(*a*), the free surface evolves from a flat initial shape. Selecting different initial shapes, including the steady shape at a finite but large value of the capillary number, has an observable effect on the gross shape of the free surface at the time of cusp formation, but a small effect on the shape of the free surface near the cusp. It seems that a nearly steady cusp forms at a finite time, and the rest of the free surface then adjusts so as to conform with the steady shape. The importance of the geometry of the cusp to the overall shape of the interface is discussed by Jeong & Moffatt (1992).

To illustrate the structure of the free surface near the cusp, in figure 6(*b*) we plot $y-y_c$ versus $x-x_c$, where (x_c, y_c) are the coordinates of the cusp, on a log–log scale. For flow due to a single point-source dipole, corresponding to $L/d=\infty$, Jeong & Moffatt (1992) found $y_c/d=-2/3$; our numerical results show that for $L/b=4.0$, the cusp is located at about $y_c/b=-0.66$. Close to the trough, and away from the undeveloped rounded part of it, the profiles in figure 6(*b*) tend to become linear with a slope that is close to the value $2/3$ predicted by Joseph and confirmed by Jeong & Moffatt. This agreement provides additional evidence that a stationary cusp is about to form. Overall, we may state with confidence that a steady cusp with the expected structure indeed forms, and tip streaming does not occur.

Koplik & Banavar (1994) carried out molecular dynamics simulations of the flow due to the counter-rotation of two cylinders in the presence of an interface separating two liquids with the same viscosity, as illustrated in figure 1(*c*). Their results showed that a cusp does not form but, instead, a drop of the upper fluid is entrained into the lower fluid, mid-way between the rollers, in a process that is reminiscent of tip streaming. In view of our results in §3, this behaviour is not surprising: whether a cusp forms or tip streaming occurs depends upon the precise structure of the incident flow that deforms the interface. More will be said about this dichotomy in the concluding section.

To examine the possibility that the viscosity of the upper fluid plays a decisive role in suppressing the formation of a cusp, we replaced the gas above the free surface in figure 1(*d*) with a liquid whose viscosity is equal to that of the lower fluid, corresponding to viscosity ratio $\lambda=1$. The evolution of the interface near the trough is illustrated in figure 6(*c*). A cusp that is even sharper than the one developing on a free surface is seen to form. Similar results were obtained for higher values of l.

Lastly, we turn to examining the effect of the point-source dipole separation L/b on the free-surface shape, with the objective of further comparing the numerical results with the analytical solution of Jeong & Moffatt corresponding to $L/b=\infty$. Our computations show that, for a certain value of Ca, the deflection and maximum curvature of the free surface at the trough at steady state are monotonically increasing functions of the ratio L/b. This is expected, since the unperturbed velocity field due

FIGURE 6. (*a*) Evolution of the free surface near the cusp in the periodic Jeong–Moffatt flow with $L/b=4$, for $Ca=\infty$. (*b*) The shape of the free surface near the cusp is described by the functional form $x-x_c=c(y-y_c)^{3/2}$ discovered by Joseph *et al.* (1991). (*c*) Evolution of the interface between two liquids with same viscosities, $\lambda=1$, in the periodic Jeong–Moffatt flow with $L/b=4$, for $Ca=\infty$.

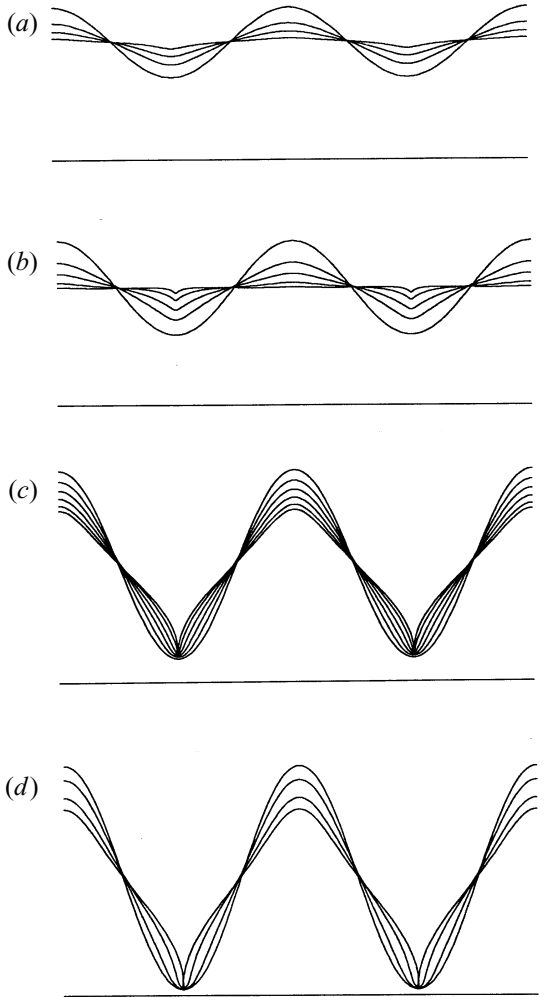

FIGURE 7. Stages in the evolution of a film resting on a horizontal wall, without surface tension, $L/H = 2$, and disturbance amplitude (*a*) $a/H = 0.20$, (*b*) 0.40, (*c*) 0.80, (*d*) 0.95.

to the singularities at the location of the free surface decays exponentially with b/L. For example, when $Ca = 0.452$, we find that κb increases from 1.0 at $L/b = 4$ to 2.1 at $L/b = 8$, where κ is the maximum curvature. In the second case, the corresponding capillary number of Jeong & Moffatt has the value $\mathscr{C} = 0.064$; using their figure 3 and their equation (3.5) we find $\kappa b = 2.2$ which is in good agreement with our numerical value for $L/b = 8$.

5. Levelling of a liquid film on a horizontal surface

The gravity- and surface-tension-driven levelling of a disturbed liquid film resting on a flat surface has been studied on many occasions, dating back to the linear analyses of Wehausen & Laitone (1960) and Orchard (1962). Further contributions include, but are not limited, to the experimental observations and numerical simulations of Degani & Gutfinger (1974, 1976), and the finite-element computations of Malamataris & Papanastasiou (1991), whose work will be discussed later in this section. Two central

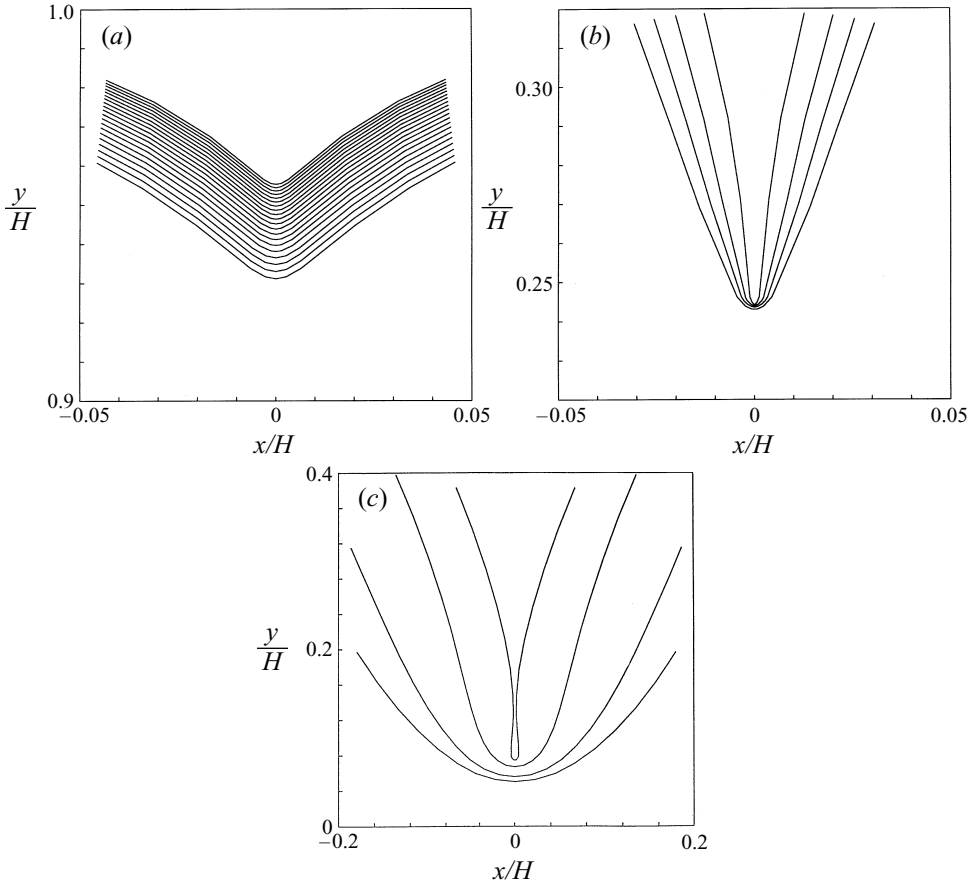

FIGURE 8. Close-up of the free surface near the critical time where a corner or a cusp forms, for vanishing surface tension, $L/H = 2$, and (*a*) $a/H = 0.40$, (*b*) 0.80, (*c*) 0.95.

objectives have been to (*a*) estimate the rate of levelling of a perturbed free surface, and (*b*) establish its dependence on the properties of the fluids.

In our numerical studies, we compute the evolution of a film with mean thickness H and density ρ, subject to a sinusoidal initial perturbation of wavelength L and amplitude a. An advanced stage in the evolution of the film with a large-amplitude perturbation is illustrated schematically in figure 1(*e*).

First, we discuss the motion in the absence of surface tension. When the amplitude is sufficiently small compared to the mean film thickness, we find that the interface levels, maintaining its sinusoidal shape. For $a/H = 0.01$, the rate of decay computed using our numerical method agrees with the linear predictions of Wehausen & Laitone and Orchard to the third significant figure. When a/H has a higher value, the deep part of the interface levels faster than the shallow part, but the interface still maintains a smooth shape, as illustrated in figure 7(*a*) for $a/H = 0.30$. Similar observations were made by previous authors. This asymmetry of the free-surface profile is attributed to the reduced magnitude of the velocity near the wall.

At larger values a/H, we find a previously unreported behaviour: in the course of levelling, the free surface develops a region of high curvature at the point of maximum depression, as illustrated in figure 7(*b*, *c*) for $a/H = 0.40$, 0.80. Details of the free-surface profile near the trough are illustrated in figure 8(*a*, *b*). Evidence that a

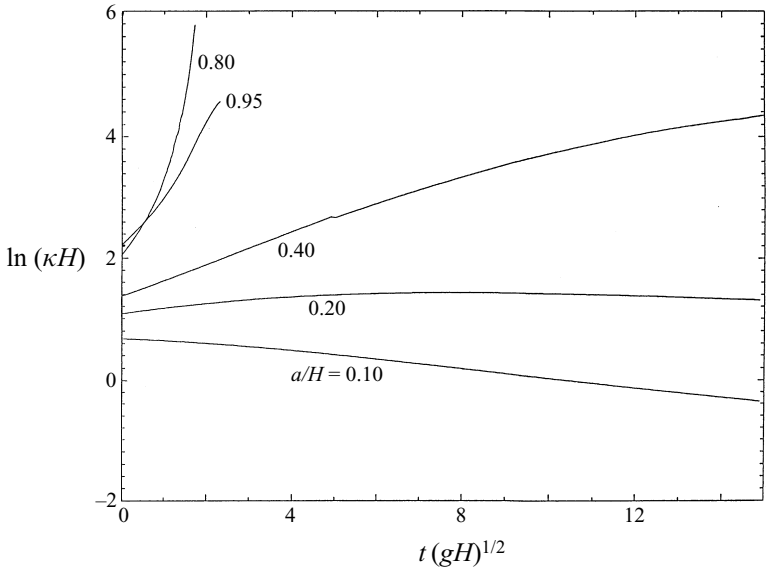

FIGURE 9. Evolution of the curvature at the trough for vanishing surface tension, $L/H = 2$, and several values of the amplitude of the initial perturbation. The continued increase of the curvature indicates the spontaneous formation of an interfacial corner or cusp.

singularity actually forms at a finite time is provided by figure 9, where we plot the curvature at the trough as a function of time on a linear–log scale. Figure 8(*a*) reveals the formation of a corner, whereas figure 8(*b*) suggests the formation of a cusp. Unfortunately, an analytical method of predicting the shape of the free surface close to the singular points could not be devised, but it is certain that it is a strong function of the current and previous structure of the flow.

For an even higher amplitude $a/H = 0.95$, the free surface engulfs a small bubble of air which is then trapped within the liquid, yielding a composite shape with a cusped interface supporting a bubble, as illustrated in figure 7(*d*) and, in more detail, in figure 8(*c*). The free surface crosses itself soon after the last stage shown in the last figure, but this is not alarming: there is nothing to keep the two parts of the free surface on either side of the plane of symmetry apart, and even replacing the inviscid gas with a slightly viscous fluid may not prevent coalescence. It is interesting to note that the composite shape described in these figures looks strikingly similar to the one predicted and plotted by Jeong & Moffatt (1992) for their model flow discussed in §4. Finally, we note that the transition from a corner to a cusp to an engulfed bubble is consistent with the crossing of the curves for $a/H = 0.80$, 0.95 in figure 9.

5.1. *Effect of surface tension*

As expected, introducing a small amount of surface tension prevents the formation of corners and cusps: the free surface maintains a smooth shape throughout the evolution. This is evident in figure 10(*a*) where we illustrate the levelling of a film with $L/H = 2$, $a/H = 0.95$, and Bond number $Bo = \rho g H^2/\gamma = 1/3$. The contrast with the evolution shown in figure 7(*d*), corresponding to the same conditions but with $Bo = \infty$, is striking.

Degani & Gutfinger (1976) and Malamataris & Papanastasiou (1991) computed the levelling of a film under a broad range of conditions. The second authors, in particular, performed an extensive set of computations using a finite-element method, and

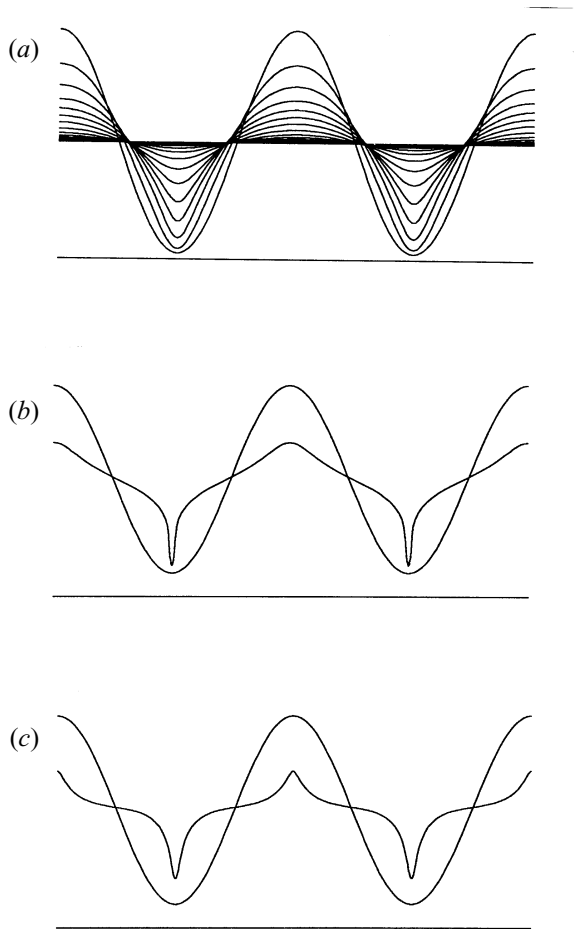

FIGURE 10. Stages in the evolution of a horizontal liquid film with $L/H = 2$, for (*a*) $a/H = 0.95$, $\lambda = 0$, and $Bo = 1/3$; (*b*) $a/H = 0.80$, $Bo = \infty$, and $\lambda = 0.10$; (*c*) $a/H = 0.80$, $Bo = \infty$, and $\lambda = 1.0$.

reported results for values of the ratio a/H as high as 0.99. Surprisingly, neither of these studies report evidence of cusp formation. Possible explanations for this absence from the results of Malamataris & Papanastasiou are: a combination of infinite capillary number and large-amplitude perturbations was not considered (the ratio a/H in their figure 20 is unspecified); inertial effects prevent cusp formation (they carry out computations at Reynolds number as low as $Re = 0.0016$); the 3×24 finite-element tesselation used by them has an inadequate resolution.

5.2. *Effect of the viscosity of the upper fluid*

Next, we examine whether replacing the inviscid gas above the liquid layer with a viscous fluid will have an important effect on singularity formation. In figure 10(*b*, *c*) we present the initial and an advanced stage in the evolution of a film with $L/H = 2$ and $a/H = 0.80$. The viscosity of the overlying fluid is, respectively, 0.10 times or equal to the viscosity of the layer. Contrasting these profiles with those shown in figure 7(*c*) illustrates that the viscosity of the upper fluid acts to widen the apparent angle of the cusp at the trough. Monitoring the evolution of the maximum curvature indicates the formation of a singularity in all cases.

A new feature is also observed: as the viscosity of the upper fluid is increased, a

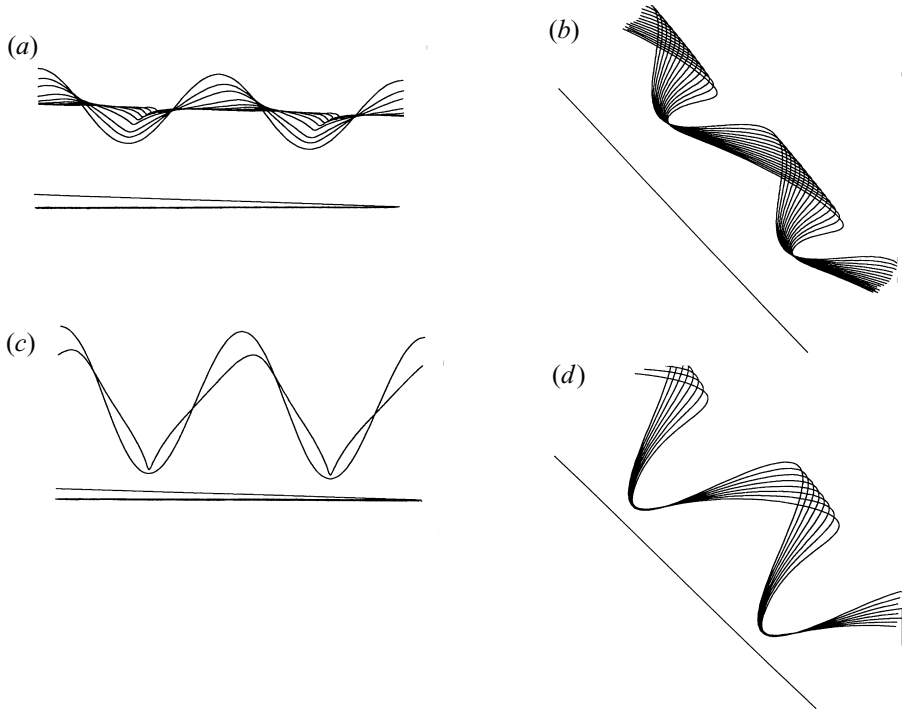

FIGURE 11. Stages in the evolution of a slightly and a substantially inclined film for $L/H = 2$, without surface tension, for (*a*) inclination angle $\theta = 0.01\pi$, $a/H = 0.40$; (*b*) $\theta = 0.25\pi$, $a/H = 0.40$; (*b*) $\theta = 0.01\pi$, $a/H = 0.80$; (*b*) $\theta = 0.25\pi$, $a/H = 0.80$.

region of high curvature develops at the maximum elevation of the levelling layer, and there is strong numerical evidence to suggest that a second singularity is likely to form there. This behaviour, however, should not be surprising: increasing the viscosity ratio λ reverses the roles of the two fluids.

5.3. *Effect of plane tilt*

In further numerical investigations, we examined the effect of a slight tilt of the plane supporting the film, that is, the effect of a gravity-driven cross-flow. At zero surface tension, we observed the formation of a corner or cusp for sufficiently large disturbance amplitudes, as shown in figure 11(*a*, *c*). The mid-plane of the cusp is now tilted with respect to the normal vector to the wall, and this suggests that the symmetry of the flow is not a necessary condition for singularity formation.

For a substantial tilting angle, we obtain the evolutions illustrated in figure 11(*b*, *d*). Unfortunately, the iterations failed to converge soon after the free-surface wave overturned, preventing us from assessing whether an interfacial singularity actually forms. Computations with perturbations of moderate amplitude, however, for example $a/L < 0.20$, proceeded without any such difficulties; and the computed rate of decay and phase velocity of perturbations with a small amplitude were in excellent agreement with the predictions of linear theories (e.g. Pozrikidis 1996, Chapter 9). In any case, the wavy flow of an inclined or vertical film is interesting in its own right. The results shown in figure 11(*b*, *d*) are believed to be the first showing the overturning of gravity waves in a flow without inertial force (Chang 1994).

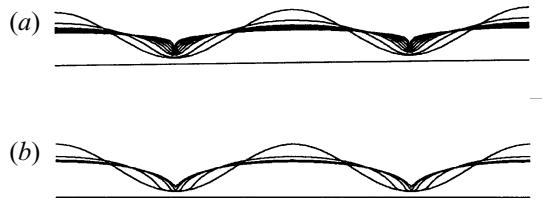

FIGURE 12. (*a*) Stages in the evolution of a film resting on a horizontal wall for vanishing surface tension, $L/H = 8$, and disturbance amplitude $a/H = 0.80$; (*b*) the corresponding evolution of the film predicted using the lubrication approximation.

5.4. *Effect of disturbance wav*

Additional corroborating evidence for unstable behaviour of a free surface with a pointed shape is provided by the numerical computations and laboratory observations of Sherwood (1984). This author observed and modelled the ejection of a liquid column from the tip of a nearly axisymmetric elongated drop in a four-roll mill apparatus. A local analysis of the steady counterpart of this flow would have presumably predicted the formation of a conical or cusped shape.

The numerical results on interfacial deformation in the generalized Jeong–Moffatt flow presented in §4 suggest that a stable *stationary* cusped configuration can indeed form at a finite time. Joseph's arguments require that both the Antanovskii and the Jeong–Moffatt steady cusps are described by the functional form $x-x_c = c(y-y_c)^{3/2}$, where x_c is the location of the cusp, the x-axis is perpendicular to the mid-plane of the cusp, and the value of the constant c depends upon the global structure of the flow. It appears then that for certain values of c the flow around the cusp is stable, whereas for other values it is unstable. The flow between two counter-rotating cylinders studied by Koplik & Banavar (1994), and the flow around the Antanovskii cusps studied in §3 of this paper must fall in the second category, although the existence of a cusped solution in the first type of flow has not been established.

The computations of the levelling of a horizontal or inclined liquid film revealed the spontaneous formation of unsteady corners and cusps in a seemingly innocuous flow. Formation of cusps – but not of corners – in unsteady flows was documented by sqeveral previous authors, as discussed in the Introduction. The levelling of the film provides us with a model flow where the whole spectrum of singular behaviour is displayed; it illustrates the continuous transition from a cornered to a cusped configuration, and the possible entrapment of a bubble with a topological singularity regarding the shape of the interface.

Perhaps more importantly, the film levelling flow provides us with an example of a viscous flow that becomes singular at a finite time, in the absence of artificial boundaries where numerical boundary conditions are imposed, and in the absence of singular points in the interior and in the exterior of the flow, including infinity. The significance of the levelling problem for painting and coating technology has been emphasized in a technical review by Quach (1973), and the present results reveal some new modes of unwanted behaviour.

Formation of singularities at the free surface of a bubble or drop in the Hele–Shaw cell has been the subject of extensive theoretical and computational investigations (e.g. Almgren 1996; Nie & Tian 1996). Howison & Richardson (1995) present a critical discussion of the similarities and differences between cusp formation in the Hele–Shaw flow and in two-dimensional Stokes flow, and our numerical results are in line with their conclusions.

I am grateful to Professor Richard Skalak for his enthusiasm in this work, and to Madhu Gopalakrishnan for providing me with useful comments on a draft. Acknowledgement is made to the Donors of the Petroleum Research Fund, administered by the American Chemical Society, for partial support of this research. Further support was provided by the National Science Foundation, and the SUN Microsystems Corporation.

REFERENCES

Almgren, R. 1996 Singularity formation in Hele–Shaw bubbles. *Phys. Fluids* **8**, 344–352.

Antanovskii, L. K. 1994*a* Quasi-steady deformation of a two-dimensional bubble placed within a potential viscous flow. *Meccanica* **29**, 27–42.

ANTANOVSKII, L. K. 1994*b* Influence of surfactants on a creeping free-boundary flow induced by two counter-rotating horizontal thin cylinders. *Eur. J. Mech.* B/*Fluids* **13**, 73–92.

ANTANOVSKII, L. K. 1994*c* A plane inviscid incompressible bubble placed within a creeping viscous flow: formation of a cusped bubble. *Eur. J. Mech.* B/*Fluids* **13**, 491–509.

BUCKMASTER, J. D. 1972 Pointed bubbles in slow viscous flow. *J. Fluid Mech.* **55**, 385–400.

CHANG, H. C. 1994 Wave evolution on a falling film. *Ann. Rev. Fluid Mech.* **26**, 103–136.

DEGANI, D. & GUTFINGER, C. 1974 Leveling of a Newtonian fluid on a horizontal surface. *Israel J. Tech.* **12**, 191–197.

DEGANI, D. & GUTFINGER, C. 1976 A numerical solution of the leveling problem. *Computers Fluids* **4**, 149–155.

HOWISON, S. D. & RICHARDSON, S. 1995 Cusp development in free boundaries, and two-dimensional slow viscous flow. *Euro. J. Appl. Maths* **6**, 441–454.

JEONG, J.-T. & MOFFATT, H. K. 1992 Free-surface cusps associated with flow at low Reynolds number. *J. Fluid Mech.* **241**, 1–22.

JOSEPH, D. D. 1992 Understanding cusped interfaces. *J. Non-Newtonian Fluid Mech.* **44**, 127–148.

JOSEPH, D. D., NELSON, J., RENARDY, M. & RENARDY, Y. 1991 Two-dimensional cusped interfaces. *J. Fluid Mech.* **223**, 383–409.

KHESHGI, H. S. 1989 Profile equations for film flows at moderate Reynolds numbers. *AIChE J.* **35**, 1719–1727.

KOPLIK, J. & BANAVAR, J. R. 1994 Fluid cusps at the molecular scale. *Phys. Fluids* **6**, 480–488.

MALAMATARIS, N. K. & PAPANASTASIOU, T. C. 1991 Unsteady free surface flows in truncated domains. *Ind. Engng Chem. Res.* **30**, 2211–2219.

NIE, Q. & TANVEER, A. 1996 The evolution of an axi-symmetric Stokes bubble with volumetric change. *Phys. Fluids.* (Submitted.)

NIE, Q. & TIAN, F. R. 1996 Singularities in Hele–Shaw flows. *SIAM J. Appl. Maths.* (Submitted.)

ORCHARD, S. E. 1962 On surface leveling in viscous liquids and gels. *Appl. Sci. Res.* A **11**, 451–464.

POZRIKIDIS, C. 1992 *Boundary Integral and Singularity Methods for Linearized Viscous Flow*. Cambridge University Press.

POZRIKIDIS, C. 1997*a* *Introduction to Theoretical and Computational Fluid Dynamics*. Oxford University Press.

POZRIKIDIS, C. 1997*b* *Numerical Computation in Science and Engineering*. Oxford University Press.

QUACH, A. 1973 Polymer coatings. Physics and mechanisms of leveling. *Ind. Engng Chem. Prod. Res. Dev.* **12**, 110–116.

RICHARDSON, S. 1968 Two-dimensional bubbles in slow viscous flow. *J. Fluid Mech.* **33**, 475–493.

RICHARDSON, S. 1973 Two-dimensional bubbles in slow viscous flow. Part 2. *J. Fluid Mech.* **58**, 115–127.

SHERWOOD, J. D. 1984 Tip streaming from slender drops in a nonlinear extensional flow. *J. Fluid Mech.* **144**, 281–295.

TANVEER, S. & VASCONELOS, G. L. 1994 Bubble-breakup in two-dimensional Stokes flow. *Phys. Rev. Lett.* **73**, 2845–2848.

TANVEER, S. & VASCONELOS, G. L. 1995 Time-evolving bubbles in two-dimensional Stokes flow. *J. Fluid Mech.* **301**, 325–344.

WEIHAUSEN, J. V. & LAITONE, E. V. 1960 Surface waves. *Handbuch der Physik* (ed. S. Flugge), **9**, 446.